Influence of Cu content on high temperature oxidation behavior of AlCoCrCu$_x$FeNi high entropy alloys (x = 0; 0.5; 1)

Juliusz Dąbrowa [a, *], Grzegorz Cieślak [b], Mirosław Stygar [a], Krzysztof Mroczka [c], Katarzyna Berent [d], Tadeusz Kulik [b], Marek Danielewski [a]

[a] AGH University of Science and Technology, Faculty of Materials Science and Ceramics, al. Mickiewicza 30, 30-059 Kraków, Poland
[b] Warsaw University of Technology, Faculty of Materials Science and Engineering, ul. Wołoska 141, 02-507 Warszawa, Poland
[c] Pedagogical University of Cracow, Institute of Technology, ul. Podchorążych 2, 30-084 Kraków, Poland
[d] AGH University of Science and Technology, Academic Centre for Materials and Nanotechnology, al. Mickiewicza 30, 30-059 Kraków, Poland

ARTICLE INFO

ABSTRACT

Studies on the oxidation behavior of high entropy alloys from the Al-Co-Cr-Cu-Fe-Ni metallic system were conducted. Three different high entropy alloys were synthesized using arc-melting method: AlCoCrFeNi, AlCoCrCu$_{0.5}$FeNi and AlCoCrCuFeNi, with their crystal structures being respectively BCC, BCC and BCC + FCC. All alloys were oxidized in the air atmosphere at temperature of 1273 K for different time periods. Basing on the thermogravimetric result, the oxidation rate of the materials decreased with the increase of Cu content and the values of parabolic constants were on the level similar to those observed in Ni-Al intermetallic alloys. In all cases the oxide scale consisted of α-Al$_2$O$_3$, which exhibited poor adhesion to the surface during the cooling process, what was especially visible in alloys with Cu addition. In all oxidized samples a tendency towards formation of the Al-depleted FCC phase directly beneath the scale was observed. The phase constitution of all materials changed significantly during the oxidation process, with multiple new phases appearing in the system.

© 2016 Elsevier Ltd. All rights reserved.

1. Introduction

High entropy alloys are currently amongst the most extensively researched metallic materials. The first concept of HEAs was presented by Yeh and Huang in 1995 [1], however it was not until 2004, when HEAs were recognized by wider public [2,3]. The most common definition of HEAs states [2,4], that they are defined as alloys with five or more principal elements. Each principal element should have a concentration between 5 and 35 at.%. The configurational entropy of such systems reaches maximum for a solution phase, what enhances the formation of solid solutions of simple crystal structures. Such an approach to the development of the alloys is radically different from the traditional one, where the alloy is based on one or two main components, with the rest of the components acting as an alloying elements.

Complexity of HEAs leads to several properties, which are not present in conventional alloys. Yeh et al. [5] summarized four main core effects of HEAs:

- thermodynamics: high entropy effects - high entropy tends to stabilize solid solution phases.
- kinetics: sluggish diffusion - diffusion coefficients are lower than in pure metals and conventional alloys.
- structure: severe lattice distortion - atoms are randomly distributed in crystal lattice, leading to lattice distortion what results in increased strength of the alloys and slower kinetics of transport processes.
- properties: cocktail effect - unexpected properties, which cannot be attributed to any of the independent components can occur.

HEAs are considered to be an extremely attractive group of materials, as they exhibit excellent physicochemical and mechanical properties, including magnetic and electrical ones. Their mechanical properties at elevated temperatures are in some cases comparable to those of conventional superalloys [4], what considering the fact that they have been developed for just about 10 years, should be viewed as a remarkable feat. Their unique properties make them suited for such applications as: heat-resistant and wear-resistant coatings, thermal-resistant coatings, materials for

* Corresponding author.
E-mail address: dabrowa@agh.edu.pl (J. Dąbrowa).

nuclear industries, structural materials for transportation and energy industries and many more [4,6]. In most of these applications, the high-temperature oxidation behavior and thermal stability are amongst the most important criteria. The high-temperature oxidation of HEAs is a relatively new topic, with most of the studies on HEAs being concentrated rather on their phase formation criteria, selection criteria, microstructure, mechanical properties and optimization of production methods. However, it seems that the development of these alloys reached a state, when new research directions can be explored, such as oxidation kinetics and diffusion studies [7—16].

Multiplicity of possible combinations of principle elements in HEAs is one of the reasons, why only a few systems had been studied in depth. Among the most popular ones are Al-Cr-Co-Fe-Ni, Co-Cr-Fe-Mn-Ni and Al-Cr-Co-Cu-Fe-Ni metallic systems [4]. Their popularity results from relatively low cost of the elements and good thermomechanical properties [2,17—21]. The oxidation behavior of these systems had been studied to some limited extent (especially for the Co-Cr-Fe-Mn-Ni system) [7,11,14—16]. However, our understanding of the oxidation behavior of the alumina-forming Al-Co-Cr-Cu-Fe-Ni alloys, especially the influence of Cu on the kinetics of oxidation, is still limited. The only previously published studies on the oxidation of Al-Co-Cr-Cu-Fe-Ni concentrated on three following alloys: $Al_8Co_{17}Cr_{17}Cu_8Fe_{17}Ni_{33}$, $Al_{23}Co_{15}Cr_{23}Cu_8Fe_{15}Ni_{15}$ and $Al_{17}Co_{17}Cr_{17}Cu_{17}Fe_{17}Ni_{17}$, with the main aim of the authors being studies on the role of Al and Cr [15].

The microstructure and phase constitution of Al-Co-Cr-Cu-Fe-Ni had been extensively studied [22—31], showing the wide range of microstructures, depending mainly on the Al and Cu content (respectively the strongest BCC and FCC formers in this particular system), with strong tendency of Cu towards segregation being reported [22,23,28]. This phenomenon may drastically alter the oxidation behavior of these alloys in comparison to the alloys from Al-Co-Cr-Fe-Ni system. Taking into account the popularity of the Al-Co-Cr-Cu-Fe-Ni high entropy alloys, studies on their oxidation behavior seem to be necessary from the point of view of potential applications.

The main aim of this study was to investigate the influence of copper content on the oxidation behavior and microstructure of AlCoCrCu$_x$FeNi (where x = 0, 0.5 and 1.0) oxidized in the air atmosphere at temperature of 1273 K.

2. Materials and methods

In our studies, three different Al-Co-Cr-Fe-Ni and Al-Co-Cr-Cu-Fe-Ni alloys were synthesized by arc-melting method using elements of high chemical purity (>99.8%), namely AlCoCrFeNi, AlCoCrCu$_{0.5}$FeNi and AlCoCrCuFeNi. Each ingot was re-melted three times to homogenize the alloy's composition and casted into the copper mold to form cylinders of 9 mm diameter. Melting and casting were conducted under high-purity argon atmosphere. The ingots were then cut using electrical discharge machining into 1 mm thick slices. Each sample was ground and polished using the standard Struers procedure, with the last polishing step being performed using 1 μm diamond paste. The alloys were examined by both optical and electron microscopy. Optical observations were performed using Carl Zeiss Axiovert 40 MAT microscope, on the samples previously etched using a mixture of 12 cm^3 - H$_2$O, 38 cm^3 - HNO$_3$, 38 cm^3 - HCl and 12 cm^3-H$_2$SO$_4$. Imaging of surface morphology and chemical analysis were performed using a FEI Versa 3D scanning electron microscope (SEM) equipped with energy dispersive X-ray spectrometer (EDS) and JEOL JSM-6610LV Scanning Electron Microscope also equipped with EDS detector. Measurements of oxidation kinetics were carried out using CI Electronics MK2-M5 balance head in laboratory air atmosphere at

temperature of 1273 K. The samples were put inside the specially formed quartz reactor (which allows undisturbed circulation of gases while protecting the sample from air movements) into already heated TGA (Thermogravimetric analysis) furnace and held at the given temperature for 100 h. The furnace was then free-cooled to minimize problems with thermal stresses and spallation. Additional samples were oxidized separately in the same thermal conditions for 100 and 500 h. Characterization of the substrate and obtained scales was performed using SEM/EDS methods and X-ray diffraction (XRD) (PANalytical X'Pert Pro PW 3710 X'Celerator). Both standard Bragg-Brentano and low angle GID methods were used (step: 0.008°, time: 80 s/step). Analysis of the obtained results were conducted using X'Pert HighScore Plus 2.0 and Crystal Impact - Match!2 software.

3. Results and discussion

3.1. Alloys microstructure

Microstructure of the as-cast materials was studied by XRD method, with the results being shown in Fig. 1. In the case of AlCoCrFeNi and AlCoCrCu$_{0.5}$FeNi alloys a pure BCC structures were observed, which is consistent with the reports of other authors [18,23,32], although sometimes a mixed BCC + FCC structure is reported for the AlCoCrFeNi alloy [17]. For the AlCoCrCuFeNi a mixed FCC + BCC structure was found, which is also consistent with previous results [23,27,28]. Observations of the etched samples using optical microscopy, presented in Fig. 2, revealed dendritic structures in all of the as-cast alloys what was expected [22]. The chemical compositions of the dendritic (D) and interdentric (ID) areas were determined using SEM/EDS method, the results are also presented in Fig. 2. As it can be seen, in the case of AlCoCrFeNi alloy a nearly identical structure to the one reported by Manzoni et al. [33] was observed, with the differences in composition between D and ID being very small. In the case of AlCoCrCu$_{0.5}$FeNi the difference between D and ID regions is more pronounced. ID is slightly enriched with Cu and Ni while having smaller Fe content. For the two-phased AlCoCrCuFeNi alloy, a clear segregation of Cu into the interdendritic regions is observed, which consists mostly of Cu and to lesser extent Al and Ni.

3.2. Morphology and phase constitution of the scales

All alloys were oxidized for 100 and 500 h. The resulting scale morphology is presented on the BSE (Backscattered electrons)
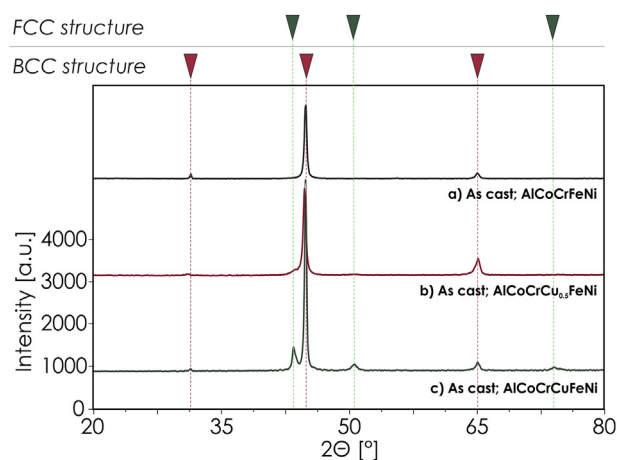

Fig. 1. The XRD spectra of the as-cast materials.

EDS quantative analysis [% at. ±0.5%] (AlCoCrFeNi)

	Al	Cr	Fe	Co	Ni
⬤	20.3	21.5	20.3	19.6	18.3
⬤	20.1	16.7	19.2	22.0	22.0

EDS quantative analysis [% at. ±0.5%] (AlCoCrCu0.5FeNi)

	Al	Cr	Fe	Co	Ni	Cu
⬤	18.5	18.6	20.5	20.8	14.4	7.3
⬤	18.8	16.1	13.5	20.9	19.2	11.6

EDS quantative analysis [% at. ±0.5%] (AlCoCrCuFeNi)

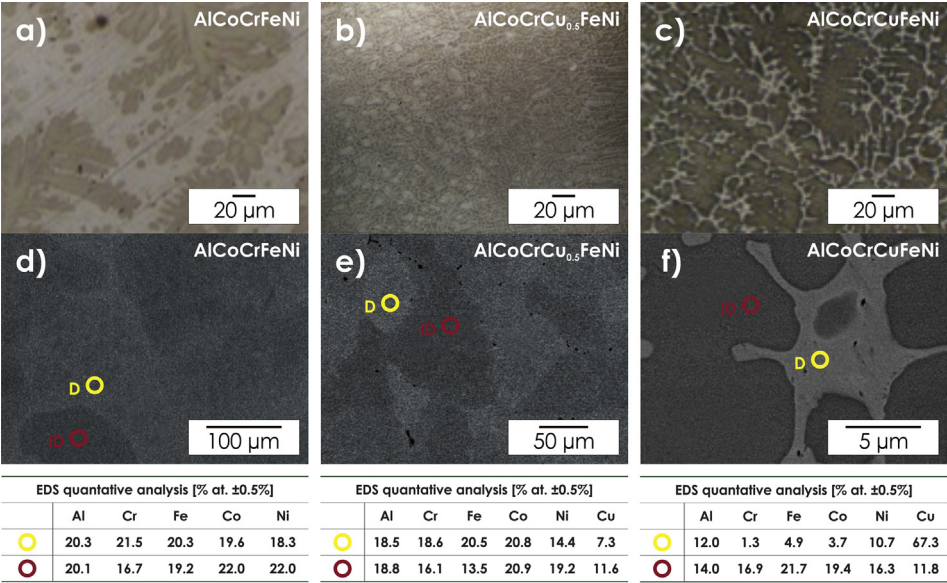|	Al	Cr	Fe	Co	Ni	Cu
⬤	12.0	1.3	4.9	3.7	10.7	67.3
⬤	14.0	16.9	21.7	19.4	16.3	11.8

Fig. 2. The results of the observations using optical a)-c) and scanning electron microscopy d)-e) of the as-cast materials: a), d) AlCoCrFeNi, b), e) AlCoCrCu0.5FeNi, c), f) AlCoCrCuFeNi. The results of EDS point analysis for each alloy are also presented.

micrographies in Fig. 3, while the results of the XRD measurements of all oxidized samples in both GID and Bragg-Brentano geometries are shown in Fig. 4.

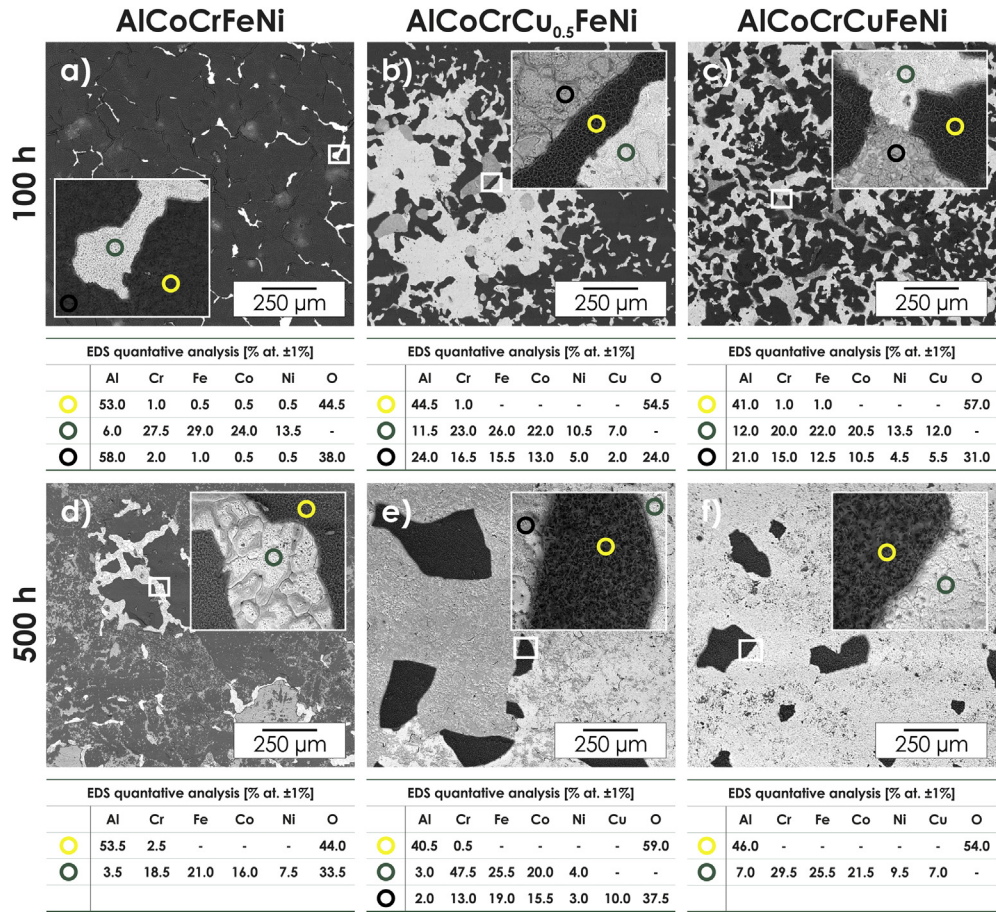For the AlCoCrFeNi alloy after 100 h of oxidation, a small

EDS quantative analysis [% at. ±1%] (AlCoCrFeNi)

	Al	Cr	Fe	Co	Ni	O
⬤	53.0	1.0	0.5	0.5	0.5	44.5
⬤	6.0	27.5	29.0	24.0	13.5	-
⬤	58.0	2.0	1.0	0.5	0.5	38.0

EDS quantative analysis [% at. ±1%] (AlCoCrCu0.5FeNi)

	Al	Cr	Fe	Co	Ni	Cu	O
⬤	44.5	1.0	-	-	-	-	54.5
⬤	11.5	23.0	26.0	22.0	10.5	7.0	-
⬤	24.0	16.5	15.5	13.0	5.0	2.0	24.0

EDS quantative analysis [% at. ±1%] (AlCoCrCuFeNi)

	Al	Cr	Fe	Co	Ni	Cu	O
⬤	41.0	1.0	1.0	-	-	-	57.0
⬤	12.0	20.0	22.0	20.5	13.5	12.0	-
⬤	21.0	15.0	12.5	10.5	4.5	5.5	31.0

EDS quantative analysis [% at. ±1%] (AlCoCrFeNi, 500 h)

	Al	Cr	Fe	Co	Ni	O
⬤	53.5	2.5	-	-	-	44.0
⬤	3.5	18.5	21.0	16.0	7.5	33.5

EDS quantative analysis [% at. ±1%] (AlCoCrCu0.5FeNi, 500 h)

	Al	Cr	Fe	Co	Ni	Cu	O
⬤	40.5	0.5	-	-	-	-	59.0
⬤	3.0	47.5	25.5	20.0	4.0	-	-
⬤	2.0	13.0	19.0	15.5	3.0	10.0	37.5

EDS quantative analysis [% at. ±1%] (AlCoCrCuFeNi, 500 h)

	Al	Cr	Fe	Co	Ni	Cu	O
⬤	46.0	-	-	-	-	-	54.0
⬤	7.0	29.5	25.5	21.5	9.5	7.0	-

Fig. 3. The BSE micrographies of the samples' morphology after 100 h of oxidation at 1273 K a)-c) and after 500 h of oxidation at 1273 K d)-e): a), d) AlCoCrFeNi, b), e) AlCoCrCu0.5FeNi, c), f) AlCoCrCuFeNi. The results of EDS point analysis for each alloy are also presented.

Fig. 4. The XRD spectra of samples oxidized for 100 h and 500 h at temperature of 1273 K measured using both Bragg-Brentano and GID geometries. The spectra of as-cast materials are also presented for reference.

were observed, although in this case the spallation is a bit more severe. For both times the XRD results are very similar, indicating that the scale consists of α-Al₂O₃. It should be noted that the oxidation of equiatomic AlCoCrFeNi alloy was also studied by Butler et al. [16] at temperature of 1050 °C for times up to 100 h. However, the applied experimental methodology, based on the discontinuous isothermal oxidation, makes it impossible to directly compare their results with the ones presented in our study. The main difference is the fact that Butler et al. reported presence of relatively high content of Cr₂O₃ (in fact, from the volumetric point of view it was a dominating oxide in the system), what may be a result of the mentioned methodology. Also, it should affect adhesion of the scale to metallic substrate, further complicating the possibility of comparison.

In the case of AlCoCrCu₀.₅FeNi and AlCoCrCuFeNi alloys after oxidation for 100 h a more intensive spallation can be observed, which intensity in general increases with the higher Cu content. Similarly to the previous alloy, all scales consist mainly α-Al₂O₃. After 500 h the spallation is even more severe, with the scale being visible on the AlCoCrCuFeNi only sporadically. While the general reason for this phenomenon is probably similar to the one proposed for the AlCoCrFeNi, there are also some differences. In the case of AlCoCrFeNi the material, which can be seen directly beneath the scale, consists of one phase, which is also supported by the cross section photos. In the case of both alloys with Cu addition it is clear that the substrate beneath the scale consists of at least two phases, which probably exhibit different CTEs, what should generate further stresses on the substrate-scale interface. Unfortunately, there is no available literature data on the CTE values of different phases in the Al-Co-Cr-Cu-Fe-Ni based high entropy alloys, however, results obtained by Daoud et al. [15] suggest that presence of the Cu-rich phase increases the CTE of the alloy as a whole.

3.3. Microstructure of the alloys after oxidation

The BSE image of the AlCoCrFeNi alloy cross-section oxidized for 100 h is presented in Fig. 5a, with corresponding XRD results being presented in Fig. 4. The relatively good adhesion of the α-Al₂O₃ scale can be observed, the scale layer is fairly uniform on the whole sample area. The main characteristics of this alloy is the presence of a continuous layer of FCC-phased Al-depleted zone thorough the whole sample, directly beneath the scale, similar to that reported for the Al₂₀Cr₂₅Co₂₅Ni₂₅Si₅ alloy by Butler et al. [7]. This is also correct according to the empirical theory of phase formation in HEAs, based on the valence electron concentration (*VEC*) [35]. The general formula is as follows:

$$VEC = \sum_{i=1}^{N} n_i(VEC_i) \tag{1}$$

where VEC_i is the *VEC* of the i-th element and n_i is the molar fration of the i-th element. In most cases the FCC phases are found to be stable at higher *VEC* (≥ 8), while the BCC phases are stable at lower *VEC* (≤ 6.87). Of course these rules are strictly empirical ones and multiple exceptions can be found [4]. The value of VEC_{Al} is 3, what makes Al a very strong BCC former. As a result, as the Al is drawn away from the substrate, the phase equilibrium shifts from the BCC phase towards the FCC. The EDS analysis indicates that the Al content within the depleted zone is about 6.2 at.%, which is also consistent with the results of Chou et al. [17] which suggest that in the Al-Co-Cr-Fe-Ni system the stable FCC phase is present up to about 10 at.% of Al content. It should be noted that the Al content within the depleted zone is uniform, as the EDS linescan through the zone does not indicate presence of a typical diffusion profile,
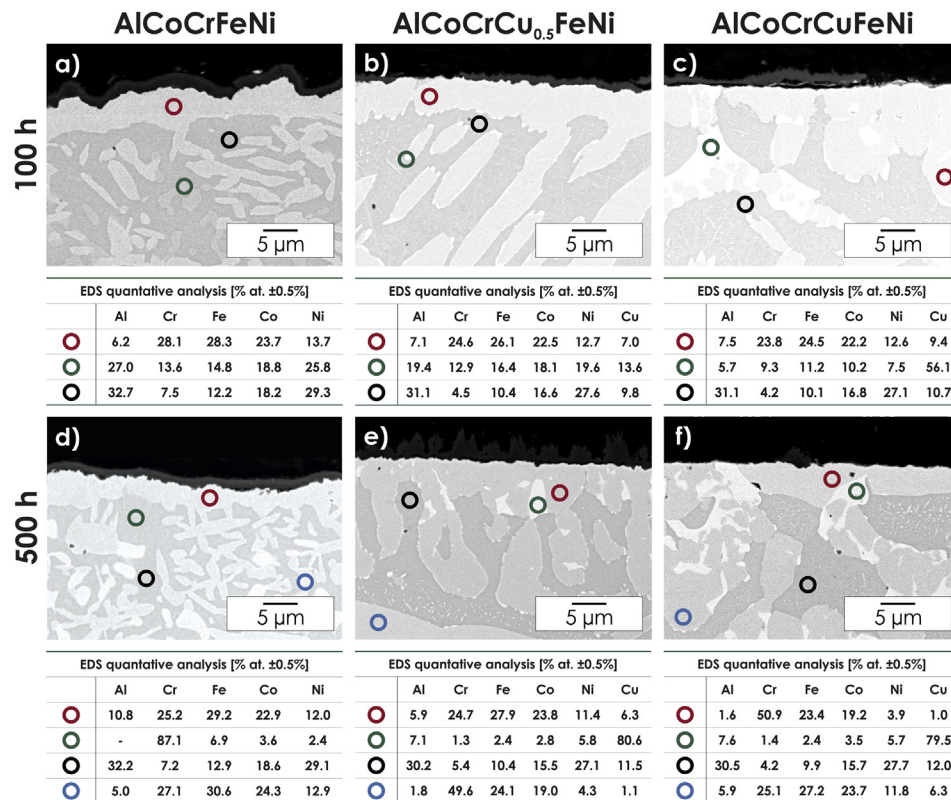
spallation of the scale can be observed in some of the sample's regions. Based on the TGA results, this process took place during cooling of the sample (what is also the case for the other two alloys) and may be a result of differences in thermal expansion coefficients (CTEs). CTEs of Al_xCoCrFeNi alloys with *x* ranging from 0 to 2, were studied by Chou et al. [17]. For these alloys, in the temperature range of 293÷773 K the CTE values were found to be in the range between 8.84 and 16.40 [10⁻⁶ K⁻¹]. However, for temperatures higher than 1000 K, values of CTE were considerably larger for all alloys, with the highest CTE of 27.26 [10⁻⁶ K⁻¹] being reported for Al₁.₅CoCrFeNi. Comparing that to the CTE of Al₂O₃, which in general does not exceed 12.00 [10⁻⁶ K⁻¹] for temperatures lower than 1273 K [34], the resulting difference can lead to the relatively high thermal stresses. For the sample oxidized for 500 h a similar results

Fig. 5. The BSE micrographies of the samples' cross-sections after 100 h of oxidation at 1273 K a)-c) and after 500 h of oxidation at 1273 K d)-e): a), d) AlCoCrFeNi, b), e) AlCoCrCu$_{0.5}$FeNi, c), f) AlCoCrCuFeNi. The results of EDS point analysis for each alloy are also presented.

what can be seen in Fig. 6. The bulk/scale interface is somewhat wavy, what may indicate that some sort of a mixed outward/inward diffusion mechanism took place in the α-Al$_2$O$_3$, with the scale growth being locally parallel to the bulk/scale interface. However, this is not supported by the adequate results for other examined alloys. The other possible explanation is that during the early stages of oxidation other phases of Al$_2$O$_3$ may form, such as θ-Al$_2$O$_3$ (in similar manner to this observed in NiAl [36]). As the alumina transforms into the more stable α phase, volumetric differences between both phases may lead to the deformation of the sample's surface, especially considering the presence of the ductile FCC phase directly beneath the scale. The bulk of the oxidized material consists of two phases. The first one is the FCC phase, which occurs in the depleted zone near the surface. The second phase displays the ordered body-centered cubic B2 structure and is significantly enriched with both Al and Ni [22,23,29], what is to be expected due to the highly negative enthalpy of mixing between these two elements [22].

The analogous results for an AlCoCrFeNi alloy oxidized for 500 h are presented in Figs. 4 and 5d. The α-Al$_2$O$_3$ scale after prolonged annealing preserves its good adhesion. In general the phase constitution is similar to the previous case, however, some differences are noticeable. The Al-depleted zone beneath the scale is still observed, although its depth does not change significantly. This fact, combined with the mentioned uniformity of Al content within the depleted zone, unfortunately, does not allow to extract any information on the Al diffusion coefficient. Two main FCC and ordered B2 phases remain the same as after 100 h of oxidation (with higher content of Cr enriched grains than in the previous case). However, the EDS analysis revealed presence of additional phases of low volumetric fraction. In Fig. 7a result of EDS mapping on the AlCoCrFeNi is presented. As it can be seen, an extremely highly Cr-

enriched grains occur within the material, with the Cr content in them being higher than 85 at.%. What is even more interesting, a number of grains within the main FCC phase seems to be enriched with Cr, what suggests that the mentioned Cr-rich grains may be a result of the transformation of FCC to disordered BCC phase (reported by Shaysultanon et al. [29]), triggered by prolonged annealing. The tendency towards enrichment of the FCC phase with Cr is also observed in other alloys and will be later discussed.

The BSE micrography of the cross-section of AlCoCrCu$_{0.5}$FeNi alloy oxidized for 100 h is presented in Fig. 5b with corresponding XRD results being presented in Fig. 4. As it was expected, the scale consists of α-Al$_2$O$_3$ and the adhesion of the scale to the substrate is significantly worse in comparison to the previous alloy, with the areas with spalled scale being clearly visible. The phase constitution after annealing changed significantly, as the alloy exhibits a dual B2+FCC microstructure. Similarly to the previous case of the AlCoCrFeNi, for the alloy with Cu addition an Al-depleted, FCC phase is observed after oxidation beneath the scale, although it does not create as continues layer as it was previously. The FCC phase is also depleted with Ni, as this element migrates into the B2 regions. As a result, the B2 phase is again Al- and Ni-enriched. The Cu is in general rather uniformly distributed through both phases, with only a marginal increase in concentration within the B2 phase. Except of the two main phases, a sub-micron precipitations of another one can be observed within the boundary regions of FCC and B2, with the EDS results indicating that this phase should be Cu-enriched.

The case of AlCoCrCu$_{0.5}$FeNi alloy oxidized for 500 h is presented in Fig. 5e. The α-Al$_2$O$_3$ scale exhibits limited adhesion and it can be clearly seen that in some regions the outer part of the scale spalled, while the inner part remained on the substrate. It is also visible, that in some regions (as presented in Fig. 5e), the scale seems to be
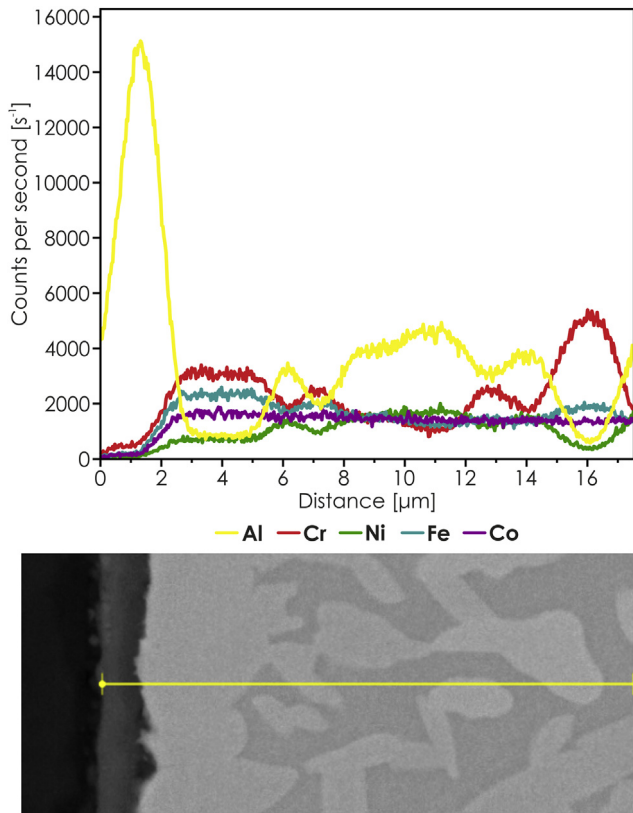
Fig. 6. The results of EDS linescan conducted in a plane perpendicular to the scale/substrate interface, on the AlCoCrFeNi sample oxidized for 500 h at temperature of 1273 K.
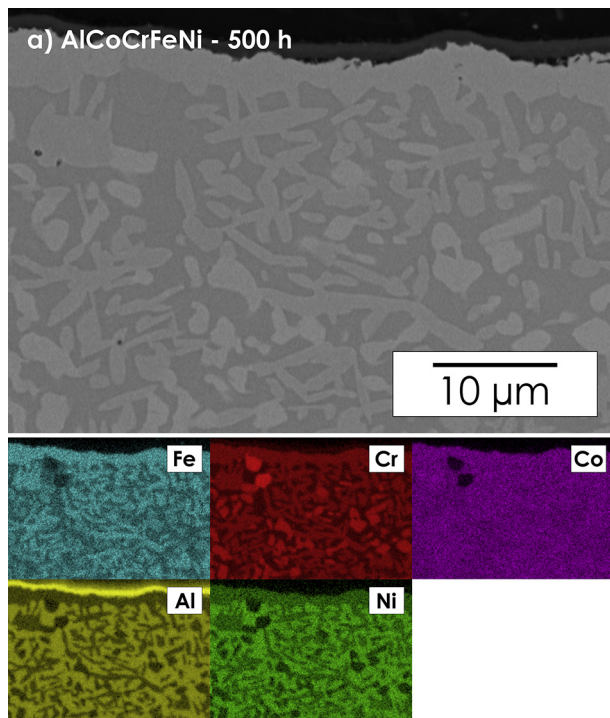

Fig. 7. Results of the EDS mapping conducted on the AlCoCrFeNi sample oxidized for 500 h at temperature of 1273 K.

thicker than in the case of AlCoCrFeNi alloy, what in opinion of the authors may be connected with the local formation of θ-Al₂O₃ characterized by bigger molar volume. This may also indicate, that the presence of Cu may influence the stability point between α- and θ-Al₂O₃, although this will require additional studies. The microstructure of the alloy after 500 h of annealing changed significantly in comparison to the microstructure after 100 h, what is also clearly visible on the XRD patterns in Fig. 4. The main difference can be attributed to the formation of new σ phase, which exhibits similar structure to the tetragonal FeCr. It can be clearly seen, that this phase is mainly a result of the transformation of the Cr, Fe and Co-rich FCC phase. The Cr content in this phase is about 50 at.%, with the Fe and Co making for the rest and splitting more or less evenly, which is consistent with the Thermo-Calc predictions made by Daoud et al. [15]. The Cu, Al and Ni content is practically negligible. While cubic-to-tetragonal transition is quite common in metallic systems (for example in NiV, NiCoV, NiFeV, FePd and CoPt [37]), such behavior has been rarely observed experimentally in Al-Co-Cr-Cu-Fe-Ni high entropy alloys. The rest of the observed phases is practically the same as after 100 h, with the Fe,Co,Cr-enriched FCC phase and Al, Ni-enriched B2 phase being still present. The previously observed precipitations of Cu-rich phase, after 500 h can be seen in a form of small grains, in which the Cu content exceeds 80 at.%. In Fig. 8 a result of EDS mapping on the AlCoCrCu₀.₅FeNi is presented, with all 3 phases being clearly distinguishable. It should be noted, that the observed cubic-to-tetragonal transition indicates, that stability of HEAs cannot be fully described basing strictly on the DTA/DSC measurements, what is the case in most of the currently published works, as the kinetics of possible phase transformations could be too slow to reveal their presence during these rather short examinations.

The BSE micrography of the cross-section of AlCoCrCuFeNi alloy oxidized for 100 h is presented in Fig. 5c with corresponding XRD results being presented in Fig. 4. The adhesion of the α-Al₂O₃ scale is similar to that on the AlCoCrCr₀.₅FeNi alloy after corresponding
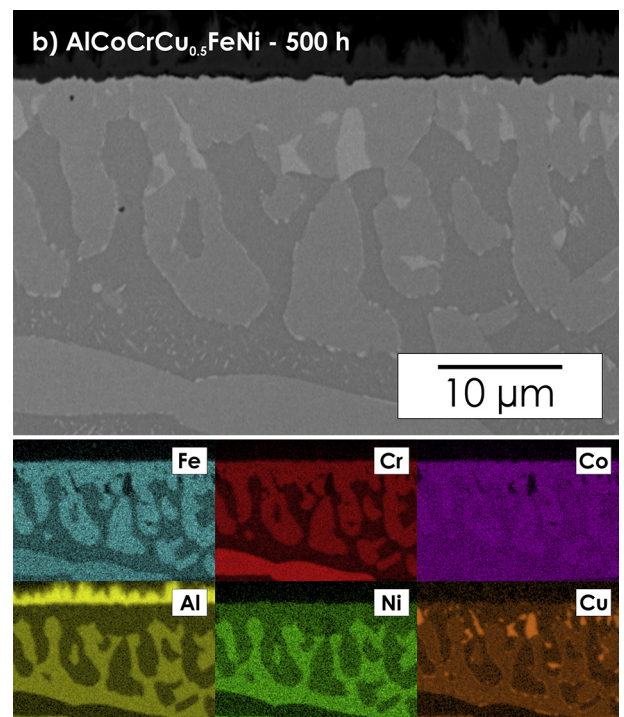

Fig. 8. Results of the EDS mapping conducted on the AlCoCrCu₀.₅FeNi sample oxidized for 500 h at temperature of 1273 K.

time. The microstructure of the alloy changed significantly as a result of annealing, with 3 different phases being clearly visible. As it was in the as-cast state, a Cu-rich FCC phase is present, however the BCC phase decomposed into the Cr, Co, Fe-rich FCC phase and Al, Ni-rich B2 phase similarly to both previous alloys.

The cross-section of AlCoCrCuFeNi alloy after 500 h of oxidation is presented in Fig. 5f. The spalling of the scale is excessive in this case, as practically no scale is visible on the sample's surface, which is consistent with the results of Daoud et al. [15]. The Cu-rich phase seems to be more evenly distributed than after 100 h, what is also visible in Fig. 9, which shows the results of EDS mapping. What is interesting, there is no difference in terms of number and types of phases in comparison to the AlCoCrCu$_{0.5}$FeNi alloy oxidized for 500 h, with the only noticeable difference being much higher content of the Cu-rich phase. It should be noted that the content of Cu within the mentioned phase is much higher than after 100 h and close to 80 at.%, what allows to say that the segregation of Cu is more pronounced after the prolonged annealing time.

Basing on the results presented in this section it can be said, that for the case of phase evolution, the Al-Co-Cr-Cu-Fe-Ni system can be divided into two subsystems: Al-Co-Cr-Fe-Ni and Cu-rich. The Al-Co-Cr-Fe-Ni equimolar subsystem evolves from BCC-phased structure into FCC Fe, Co, Cr-enriched phase and Al, Ni-enriched ordered B2 phase. The stability of the second phase is rather high, with no dramatic changes of composition being observed between 100 h and 500 h of annealing, however the FCC phase further evolves towards higher Cr enrichment, what after prolonged annealing leads to formation of the Fe, Co, Cr-based σ phase. The evolution of Cu-rich subsystem seems to be independent from the other components, and leads to further depletion of the Cu-enriched grains from other components, with the final result being grains of about 80% at. Cu content. The eventual interactions between both subsystems during long-time annealing should be further investigated.

To conclude this section it should be said, that the term of "high

Fig. 9. Results of the EDS mapping conducted on the AlCoCrCuFeNi sample oxidized for 500 h at temperature of 1273 K.

entropy alloys high-temperature oxidation studies" is somehow misleading, as basing on our results and results of other authors [7] it can be said, that for the most high entropy alloys oxidized for prolonged times the investigated systems are in fact multi-phased, including the HEAs solid-state solutions as just one of the components. Their overall phase composition is far from the as-cast state. In the opinion of the authors more effort should be put on the studies of HEAs after prolonged annealing, which is more representative of the actual state of these materials in real applications. Basing on our results it is safe to say, that focusing on the as-cast state materials may be misleading, as the evolution of HEAs' microstructures take place for several hundreds of hours and as of today it is not clear how these processes influence properties of the alloys of interest.

3.4. Oxidation kinetics and mechanism

Results of the oxidation kinetics measurements are presented in Fig. 10 using both normal and parabolic plots. As shown in this figure, the oxidation kinetics at 1273 K for all studied alloys were approximated using a single-stage parabolic law in a form:

$$\left(\frac{\Delta m}{S}\right)^2 = 2k_p t + C, \qquad (2)$$

although a small deviations from the parabolic law are observed during early stages of oxidation (especially for the AlCoCrFeNi alloy). In all cases there is no indication that during the measurements spallation took place, as there are no noticeable drop-offs on the mass gain curve during the isothermal period.

The k_p values for the AlCoCrFeNi, AlCoCrCu$_{0.5}$FeNi and AlCoCrCuFeNi alloys are respectively: $9.39 \cdot 10^{-13}$, $3.40 \cdot 10^{-13}$ and $8.00 \cdot 10^{-14}$ [g^{2}cm^{-4}s^{-1}]. A clear correlation of the results can be seen: the higher the copper content, the lower the k_p value.

Extremely important and interesting here is the comparison of the oxidation rates of HEAs with alumina-forming intermetallics and conventional alloys. The values of the parabolic constants k_p measured for the exemplary alloys by different authors are presented in Table 1 [38–43]. It should be noted that some of these results were obtained for alloys already optimized for high-temperature applications. Even though, the oxidation kinetics of the examined HEAs are comparable to those of NiAl-based alloys and Ni-Cr-Al and superior to the FeAl- and TiAl-based alloys. This is also supported by the results obtained by Butler et al. [7] for alumina-forming Al$_{20}$Cr$_{25}$Co$_{25}$Ni$_{25}$Si$_5$, for which a $k_p = 5.10 \cdot 10^{-15}$ [g^{2}cm^{-4}s^{-1}] was determined (however it should be noted that the measurements were performed using discontinuous method). The biggest drawback of the examined alloys from the point of view of possible applications, was relatively weak adhesion of the scale to the substrate. However, it can possibly be improved by the usage of alloying addition of reactive elements such as Y, Zr or Hf [44–46]. Basing on these facts it can be stated that alumina-forming HEAs have a great potential in high-temperature applications and a great effort should be put on further studies of their oxidation behavior and optimization of their composition.

Butler et al. [7] postulated that the mechanism of Al-Cr-Ni containing HEAs can be described basing on the Giggins-Pettit theory of Ni-Cr-Al alloys oxidation [39]. It is an empirically based theory that divides Ni-Cr-Al alloys into 3 regimes, basing on the oxide maps:

- Group I corresponds to dilute alloys in which Cr and Al concentrations are too low to establish continuous Cr$_2$O$_3$ or Al$_2$O$_3$ scales. Instead, the external scales consist of NiO plus Ni$_2$Cr$_2$O$_4$

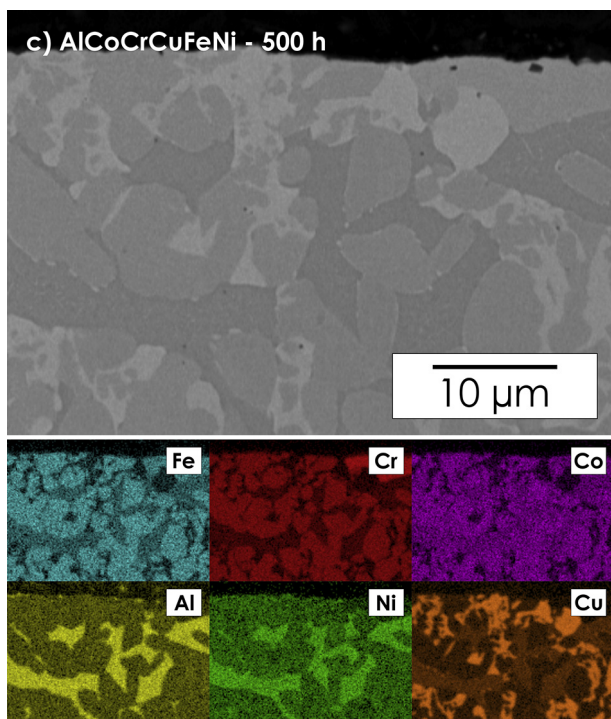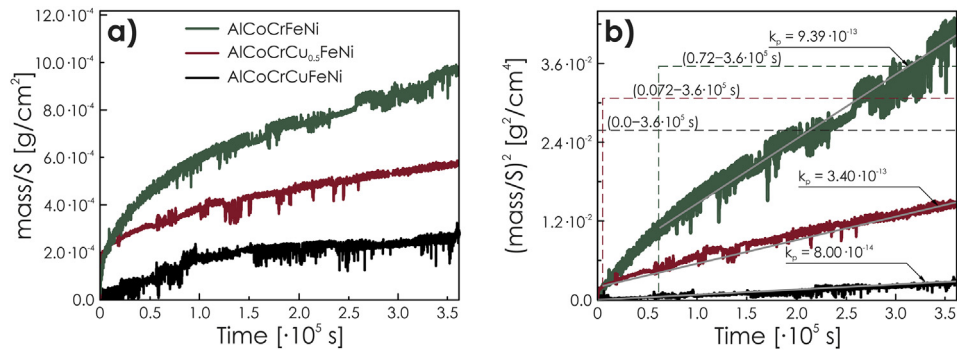**Fig. 10.** Mass gain curves measured of all materials oxidized at temperature of 1273 K for 100 h presented on a) normal b) parabolic plot. The k_p values [g²·cm⁻⁴·s⁻¹] with the time ranges for which they were determined are also visible.

Table 1
The values of the parabolic constants measured for the exemplary alumina-forming alloys by different authors.

Alloy	k_p [g²cm⁻⁴ s⁻¹]	Temperature [K]	Reference
AlCoCrFeNi	$9.4 \cdot 10^{-13}$	1273	This work
AlCoCrCu$_{0.5}$Ni	$3.4 \cdot 10^{-13}$	1273	
AlCoCrCuFeNi	$8.0 \cdot 10^{-14}$	1273	
Ni-50Al-0.05Zr	$3.8 \cdot 10^{-15}$	1273	[38]
Ni-50Al	$3.1 \cdot 10^{-14}$	1273	
Ni-46.5Al-0.05Zr	$4.9 \cdot 10^{-14}$	1273	
Ni-43Al-0.05Zr	$1.2 \cdot 10^{-13}$	1273	
Ni-39Al-0.05Zr	$1.3 \cdot 10^{-13}$	1273	
Ni-36.5Al-0.05Zr	$1.0 \cdot 10^{-13}$	1273	
Ni-34Al-0.05Zr	$4.3 \cdot 10^{-14}$	1273	
Ni-30Al-0.05Zr	$2.6 \cdot 10^{-13}$	1273	
Ni-30Al	$6.7 \cdot 10^{-14}$	1273	
Ni-5Cr-6Al	$1.4 \cdot 10^{-14}$	1273	[39]
NiAl-7Cr	$3.6 \cdot 10^{-14}$	1273	[40]
NiAl-15Cr	$7.1 \cdot 10^{-14}$	1273	
NiAl-34Cr	$1.4 \cdot 10^{-13}$	1273	
Ni-50Al (α-Al$_2$O$_3$)	$1.1 \cdot 10^{-14}$	1273	[41]
Ni-50Al (θ-Al$_2$O$_3$)	$1.1 \cdot 10^{-12}$	1273	
FeAl(Zr,B)	$4.4 \cdot 10^{-13}$	1273	[42]
FeAl(Hf)	$3.1 \cdot 10^{-13}$	1273	
FeAl(Hf,B)	$2.5 \cdot 10^{-13}$	1273	
Ti-26Al	$2.2 \cdot 10^{-9}$	1248	[43]
Ti-34Al	$7.0 \cdot 10^{-10}$	1248	
Ti-49Al	$9.9 \cdot 10^{-11}$	1248	

and Ni$_2$Al$_2$O$_4$ spinel phases coupled with internal oxidation of Al.

- Group II corresponds to alloys with large enough Cr concentrations, but relatively low Al concentrations, that results in selective oxidation of Cr, which forms external Cr$_2$O$_3$ scale. The formation of internal Al$_2$O$_3$ subscale proceeds as a result of internal oxidation.
- Group III corresponds to alloys containing large enough Al concentration to promote the selective oxidation of Al, that results in formation of external Al$_2$O$_3$ scale.

Each of the groups is characterized by different sequence of transport mechanisms, which lead to different compositions of the scales. The schematic of those sequences is presented in Fig. 11.

All examined alloys from our work, due to the relatively high Al content, can be assigned to the group III in the Giggins-Pettit theory. As it was mentioned before, in all cases the scale consisted only of α-Al$_2$O$_3$. That, however, does not make the whole argument invalid, as the other scale elements predicted by the theory may be detectable only for a very short oxidation times or not detectable at all (for example the Cr$_2$O$_3$ on the Al$_{20}$Cr$_{25}$Co$_{25}$Ni$_{25}$Si$_5$ alloy oxidized at 1323 K is not visible for annealing times higher than 96 h and the

Ni(Cr,Al)$_2$O$_4$ spinel was not detected [7]). The determination of scale composition is also difficult in our case due to its spallation. The mechanism of diffusion during the oxidation process is not completely clear. However, basing on the generally weak adhesion of the scale, as well as results of other authors concerning HEAs oxidation, it can be assumed that in all three examined alloys the scale was formed mainly as a result of Al outward diffusion, which is consistent with the group III mechanism visible in Fig. 11. In general, the results confirm the assumptions of Butler et al. [7]. However, further studies will be needed to fully investigate the sequence of oxide formation at the early stages of oxidation and to determine the mechanisms during this period.

4. Conclusions

The studies on the oxidation behavior of high entropy alloys from the Al-Co-Cr-Cu-Fe-Ni were conducted. Three different alloys were synthesized using arc-melting method: AlCoCrFeNi, AlCoCrCu$_{0.5}$FeNi and AlCoCrCuFeNi. All studied alloys were oxidized in the air atmosphere at 1273 K for 100 and 500 h.

1. In all cases the scale consisted of α-Al$_2$O$_3$ which adhesion worsens with the increase of Cu content from relatively good for AlCoCrFeNi to the spallation of almost whole scale for AlCoCrCuFeNi after 500 h of oxidation.
2. As a result of oxidation a BCC AlCoCrFeNi alloy changed its structure to dual-phased: Co, Cr, Fe-enriched FCC and Al, Ni-enriched B2 phase. The FCC phase formed an Al-depleted, continuous layer directly beneath the scale. After 500 h a tendency towards further Cr enrichment of FCC phase occurred.
3. After oxidation of the BCC-phased AlCoCrCu$_{0.5}$FeNi alloy a change in the phase composition was observed, with formation of similar phases as in AlCoCrFeNi: Co, Cr, Fe-enriched FCC and Al, Ni-enriched B2 phase, with the Cu being rather evenly distributed in the whole structure. A small precipitations of the third, Cu-rich phase were observed. After 500 h of oxidation the microstructure changed drastically, with the transformation of part of FCC phase to the (Fe, Co)Cr σ phase, accompanied by growth of the Cu-rich (up to 80 at.%) grains.
4. The behavior of the BCC + FCC AlCoCrCuFeNi high entropy alloy during oxidation was very similar to the AlCoCrCu$_{0.5}$FeNi, with the most noticeable difference being much higher content of the Cu-rich phase. During the annealing it is noticeable that the Cu content within this phase increased from about 55 at.% after 100 h to 80 at.% after 500 h of oxidation.
5. The obtained results show that the microstructure of the examined HEAs after 500 h of oxidation is still far from the not
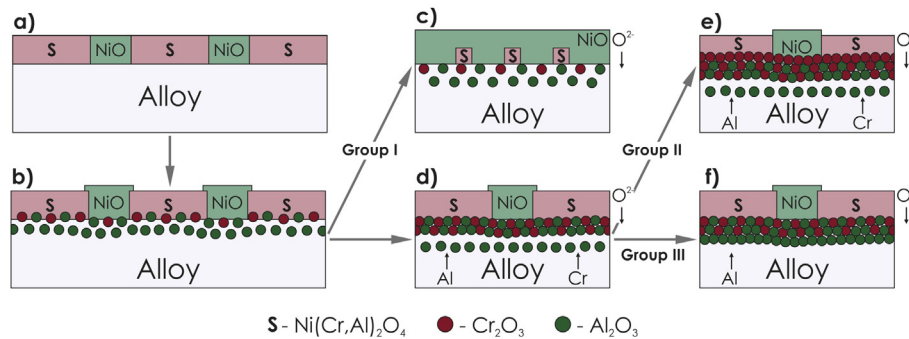
Fig. 11. Schematic diagram illustrating the oxidation mechanisms of Ni-Cr-Al alloys based on the original figure by Giggins et al. [39]. The diffusion directions are presented by the arrows. a) Conversion of a thin alloy surface layer to oxide by rapid uptake of oxygen. The oxide phases formed are determined by the composition of the alloy. b) Diffusion within the alloy results in the formation of a Cr_2O_3 and Al_2O_3 subscale beneath the external scale. c) For alloys with low chromium and aluminum concentrations, the subscale cannot become continuous and NiO in the external scale predominates (Group I). d) For alloys with higher chromium and aluminum concentrations, the subscale becomes continuous but aluminum is still oxidized internally beneath this duplex internal oxide layer. e) For alloys with smaller aluminum concentrations, the aluminum continues to be oxidized internally and the continuous duplex layer is enriched in chromium (Group II). f) For alloys with larger aluminum concentrations, the Al_2O_3 subscale zone becomes continuous beneath the duplex oxide layer (Group III).

yet defined equilibrium, signaling the necessity of long term annealing studies on the HEAs' stability.

6. It was found that the oxidation kinetics of the alloys strongly depended on the Cu content - the higher it was, the lower values of parabolic constants k_p were observed. The values of k_p were comparable to those of NiAl and NiCrAl alloys. The mechanism of oxidation was similar to that predicted by Giggins-Pettit theory, with the scale formation occurring mostly via outward diffusion of Al.

Acknowledgements

References

[1] K.H. Huang, J.W. Yeh, A Study on Multicomponent Alloy Systems Containing Equal-mole Elements, National Tsing Hua University, Hsinchu, 1996 (M.S. thesis).

[2] J.W. Yeh, S.K. Chen, S.J. Lin, J.Y. Gan, T.S. Chin, Nanostructured high-entropy alloys with multiple principal elements: novel alloy design concepts and outcomes, Adv. Eng. Mater. 6 (2004) 299—303.

[3] B. Cantor, I.T. Chang, P. Knight, A.J. Vincent, Microstructural development in equiatomic multicomponent alloys, Mater. Sci. Eng. A 375—377 (2004) 213—218.

[4] Y. Zhang, T.T. Zuo, Z. Tang, M.C. Gao, K.A. Dahmen, P.K. Liaw, Z.P. Lu, Microstructures and properties of high-entropy alloys, Prog. Mater. Sci. 61 (2014) 1—93.

[5] J.W. Yeh, Recent progress in high-entropy alloys, Ann. de Chimie - Sci. des Materiaux 31 (2006) 633—648.

[6] D.B. Miracle, J.D. Miller, O.N. Senkov, C. Woodward, M.D. Uchic, J. Tiley, Exploration and development of high entropy alloys for structural applications, Entropy 16 (2014) 494—525.

[7] T.M. Butler, J.P. Alfano, R.L. Martens, M.L. Weaver, High temperature oxidation behavior of Al-Co-Cr-Ni-(Fe or Si) multicomponent high-entropy alloys, JOM 16 (2015) 246—259.

[8] K.Y. Tsai, M.H. Tsai, J.W. Yeh, Sluggish diffusion in Co-Cr-Fe-Mn-Ni high-entropy alloys, Acta Mater. 61 (2013) 4887—4897.

[9] J. Dąbrowa, W. Kucza, G. Cieślak, T. Kulik, M. Danielewski, J.W. Yeh, Interdiffusion in the FCC-structured Al-Co-Cr-Fe-Ni high entropy alloys: experimental studies and numerical simulations, J. Alloys Compd. 674 (2016) 445—462.

[10] C.M. Liu, H.M. Wang, S.Q. Zhang, H.B. Tang, A.L. Zhang, Microstructure and oxidation behavior of new refractory high entropy alloys, J. Alloys Compd. 583 (2014) 162—169.

[11] L.H. Hong, H. Zhang, Q.H. Tang, J.C. Wen, P.Q. Dai, High Temperature oxidation behavior of $Al_{0.5}$CrCoFeNi high entropy alloy, Rare metal Mater. Eng. 44 (2015) 424—428.

[12] S.T. Chen, W.H. Tang, Y.F. Kuo, S.Y. Chen, C.H. Tsau, T.T. Shun, J.W. Yeh, Microstructure and properties of age-hardenable Al_xCrFe$_{1.5}$MnNi$_{0.5}$ alloys, Mater. Sci. Eng. A 527 (2010) 5818—5825.

[13] M.H. Chuang, M.H. Tsai, W.R. Wang, S.J. Lin, J.W. Yeh, Microstructure and wear behavior of Al_xCo$_{1.5}$CrGeNi$_{1.5}$Ti$_y$ high-entropy alloys, Acta Mater. 59 (2011) 6308—6317.

[14] G.R. Holcomb, J. Tylczak, C. Carney, Oxidation of CoCrFeMnNi high entropy alloys, JOM 67 (2015) 2326—2339.

[15] H.M. Daoud, A.M. Manzoni, R. Völkl, N. Wanderka, U. Glatzel, Oxidation behavior of Al_8Co$_{17}$Cr$_{17}$Cu$_8$Fe$_{17}$Ni$_{33}$, Al_{23}Co$_{15}$Cr$_{23}$Cu$_8$Fe$_{15}$Ni$_{15}$ and Al_{17}Co$_{17}$/cr$_{17}$Cu$_{17}$Fe$_{17}$Ni$_{17}$ compositionally complex alloys (High-Entropy alloys) at elevated temperatures in air, Adv. Eng. Mater. 17 (2015) 1134—1141.

[16] T.M. Butler, M.L. Weaver, Oxidation behavior of arc melted AlCoCrFeNi multi-component high entropy alloys, J. Alloys Compd. 674 (2016) 229—244.

[17] H.P. Chou, Y.S. Chang, S.K. Chen, J.W. Yeh, Microstructure, thermophysical and electrical properties in Al_xCoCrFeNi ($0\leq x\leq 2$) high entropy alloys, Mater. Sci. Eng. B 163 (2009) 184—189.

[18] Y.F. Kao, T.J. Chen, S.K. Chen, J.W. Yeh, Microstructure and mechanical property of as-cast, -homogenized, and -deformed AlxCoCrFeNi ($0\leq x\leq 2$) high-entropy alloys, J. Alloys Compd. 488 (2009) 57—64.

[19] C.J. Tong, M.R. Chen, S.K. Chen, J.W. Yeh, T.T. Shun, S.J. Lin, S.Y. Chang, Mechanical performance of the AlCoCrCuFeNi High-Entropy alloy system with multiprincipal elements, Metallurgical Mech. Trans. A 36A (2005) 1263—1271.

[20] A.J. Zaddach, C. Niu, C.C. Koch, D.L. Irving, Mechanical properties and stacking fault energies of NiFeCrCoMn high-entropy alloy, JOM 65 (2013) 1780—1789.

[21] F. Otto, A. Dlouhy, C.H. Somsen, H. Bei, G. Eggeler, E.P. George, The influences of temperature and microstructure on the tensile properties of a CoCrFeMnNi high-entropy alloy, Acta Mater. 61 (2013) 5743—5755.

[22] S. Singh, N. Wanderka, B.S. Murty, U. Glatzel, J. Banhart, Decomposition in multi-component AlCoCrCuFeNi high-entropy alloy, Acta Mater. 59 (2011) 182—190.

[23] C.C. Tung, J.W. Yeh, T. Shun, S.K. Chen, Y.S. Huang, H.C. Chen, On the elemental effect of AlCoCrCuFeNi high-entropy alloy system, Mater. Lett. 61 (2007) 1—5.

[24] J.W. Aveson, A. Bhowmik, B.D. Conduit, H.J. Stone, On the entropic stabilization of an $Al_{0.5}$CrFeCoNiCu high entropy alloy, Intermetallics 54 (2014) 148—153.

[25] A. Manzoni, H. Daoud, S. Mondal, S. van Smaalen, R. Völkl, U. Glatzel, N. Wanderka, Investigation of phases in Al_{23}Co$_{15}$Cr$_{23}$Cu$_8$Fe$_{15}$Ni$_{16}$ and Al_8Co$_{17}$Cr$_{17}$Cu$_8$Fe$_{17}$Ni$_{33}$ high entropy alloys and comparison with equilibrium phases predicted by Therm-Calc, J. Alloys Compd. 552 (2013) 430—436.

[26] C. Ng, S. Guo, J. Luan, S. Shi, C.T. Liu, Entropy-driven phase stability and slow diffusion kinetics in an $Al_{0.5}$CoCrCuFeNi high entropy alloy, Intermetallics 31 (2012) 165—172.

[27] C.J. Tong, Y.L. Chen, S.K. Chen, J.W. Yeh, T.T. Shun, C.H. Tsau, S.J. Lin, S.Y. Chang, Microstructure characterization of Al_xCoCrCuFeNi high-entropy alloy system with multiprincipal elements, Merallurgical Mater. Trans. A 36A (2005) 881—893.

[28] L.H. Wen, H.C. Kou, J.S. Li, H. Chang, X.Y. Xue, Zhou, Effect of aging temperature on microstructure and properties of AlCoCrCuFeNi high-entropy alloy, Intermetallics 17 (2009) 266—269.

[29] D.G. Shaysultanov, N.D. Stepanov, A.V. Kuznetsov, G.A. Salishchev, O.N. Senkov, Phase Composition, Superplastic, Behavior of a wrought AlCoCrCuFeNi high-entropy alloy, JOM 65 (2013) 1815—1828.

[30] V. Dolique, A.L. Thomann, P. Brault, Y. Tessier, P. Gillon, Complex structure/composition relationship in thin films of AlCoCrCuFeNi high entropy alloy, Mater. Chem. Phys. 117 (2009) 142—147.

[31] V. Dolique, A.L. Thomann, P. Brault, Y. Tessier, Gillon, Thermal stability of AlCoCrCuFeNi high entropy alloy thin films studied by in-situ XRD analysis, Surf. Coatings Technol. 204 (2010) 1989—1992.

[32] Y.P. Wang, B.S. Li, M.X. Ren, C. Yang, H.Z. Fu, Microstructure and compressive properties of AlCrFeCoNi high entropy alloy, Mater. Sci. Eng. A 491 (2008)

154—158.

[33] A. Manzoni, H. Daoud, R. Völkl, U. Glatzel, N. Wanderka, Phase separation in equiatomic AlCoCrFeNi high-entropy alloy, Ultramicroscopy 132 (2013) 212—215.

[34] A.M. Huntz, L. Maréchal, B. Lesage, R. Molins, Thermal expansion coefficient of alumina films developed by oxidation of a FeCrAl alloy determined by a deflection technique, Appl. Surf. Sci. 252 (2006) 7781—7787.

[35] S. Guo, N. Chun, L. Hian, C.T. Liu, Effect of valence electron concentration on stability of fcc or bcc phase in high entropy alloys, J. Appl. Phys. 109 (2011) 103505.

[36] G.C. Rybicki, J.L. Smialek, Effect of the θ-α-Al_2O_3Transformation on the oxidation behavior of β-NiAl+Zr, Oxid. Metals 31 (1989) 275—304.

[37] H. Zapolsky, S. Ferry, X. Sauvage, D. Blavette, L.Q. Chen, Kinetics of cubic-to-tetragonal transformation in Ni-V-X alloys, Philos. Mag. 90 (2010) 337—355.

[38] J. Doychak, J.L. Smialek, C.A. Barrett, The oxidation of Ni-Rich Ni-Al in-termetallics, in: T. Grobstein, J. Doychak (Eds.), Oxidation of High-Temperature Intermetallics, The Minerals, Metals & Materials Society, Penn-sylvania, 1988, pp. 41—56.

[39] C.S. Giggins, F.S. Pettit, Oxidation of Ni-Cr-Al alloys between 1000 °C and

[40] H.J. Grabke, Oxidation of NiAl and FeAl, Intermetallics 7 (1999) 1151—1158.

[41] M.W. Brumm, H.J. Grabke, The oxidation behaviour of NiAl - I. Phase trans-formations in the alumina scale during oxidation of NiAl and NiAl-Cr alloys, Corros. Sci. 33 (1992) 1677—1690.

[42] J.L. Smialek, J. Doychak, D.J. Gaydosh, Oxidation behavior of FeAl+Hf, Zr, B, in: T. Grobstein, J. Doychak (Eds.), Oxidation of High-Temperature Intermetallics, the Minerals, Metals & Materials Society, Pennsylvania, 1988, pp. 83—96.

[43] G. Welsch, A.I. Kahveci, Oxidation behavior of Titanium aluminide alloys, in: T. Grobstein, J. Doychak (Eds.), Oxidation of High-Temperature Intermetallics, the Minerals, Metals & Materials Society, Pennsylvania, 1988, pp. 207—218.

[44] J. Jedliński, S. Mrowec, The influence of implanted yttrium on the oxidation behavior of β-NiAl, Mater. Sci. Eng. 87 (1987) 281—287.

[45] C.A. Barrett, Effect of 0.1 at. % zirconium on the cyclic oxidation resistance of β-NiAl, Oxid. Metals 30 (1988) 361—390.

[46] S. Taniguchi, T. Shibata, H. Tsuruoka, Isothermal oxidation behavior of Ni_3Al-0.1B base alloys containing Ti, Zr, or Hf additions, Oxid. Metals 26 (1986) 1—17.

1200 °C, J. Electrochem. Soc. 118 (1971) 1782—1790.